J|A|C|S
ARTICLES
Published on Web 02/07/2007

Surface Chemistry of Aerosolized Silicon Nanoparticles: Evolution and Desorption of Hydrogen from 6-nm Diameter Particles

Jason Holm† and Jeffrey T. Roberts*,‡

Contribution from the Departments of Mechanical Engineering and Chemistry, University of Minnesota, Minneapolis, Minnesota 55455

Received August 14, 2006; E-mail: roberts@chem.umn.edu

Abstract: The surface chemistry of pristine, 6-nm silicon nanoparticles has been investigated. The particles were produced in an RF plasma and studied using a tandem differential mobility analysis apparatus, Fourier transform infrared spectroscopy (FTIR), time-of-flight secondary ion mass spectrometry (ToF-SIMS), and transmission electron microscopy. Particles were extracted from the plasma, which operates at ~20 Torr, into an atmospheric pressure aerosol flow tube, and then through a variable-temperature furnace that could be adjusted between room temperature and 1200 °C. DMA measurements show that freshly generated silicon particles shrink with heating, with particle diameters decreasing by ~0.25 nm between 350 and 400 °C. FTIR results indicate that freshly generated particles are primarily covered with SiH_2 groups and smaller amounts of SiH and SiH_3. Spectra recorded as a function of heating temperature indicate that the amount of surface hydrogen, as measured by the intensity of modes associated with SiH, SiH_2, and SiH_3, decreases with heating. ToF-SIMS measurements also suggest that hydrogen desorbs from the particles surfaces over the same temperature range that the particles shrink.

Introduction

Silicon nanoparticles are receiving attention for diverse applications such as luminescent devices,[1] nontoxic biological markers,[2] and single particle transistors,[3] and for improving photovoltaic conversion in hydrogenated, amorphous silicon (a-Si:H) solar cells.[4] Because many proposed applications rely on particle size control, accurately monitoring, manipulating, and preserving individual particle sizes are all of critical importance. Additionally, many applications require specifically functionalized particle surfaces to elicit desired characteristics or responses. Knowledge of the pristine nanoparticle surface chemistry is therefore of interest. By determining the particle surface chemistry, one may also gain valuable insight into appropriate functionalization techniques and materials. For instance, hydrosilylation is well-established as a method for providing organic functionalization to the surface of a silicon wafer.[5−8] Because hydrosilylation involves the reaction of an organic modifying agent with one or more surface Si−H bonds, the nature of a pristine surface, and in particular the coverage and state of adsorbed hydrogen, will partly determine whether hydrosilylation is an appropriate functionalization strategy.

Particle mobility diameter changes in the aerosol phase are often measured by tandem differential mobility analysis (TDMA).[9] The technique has frequently been used to evaluate size distribution changes due to volatization of atmospheric aerosols[10] and, more recently, growth of silicon nanoparticles due to thermal oxidation[11] and uptake of organic molecules on silicon nanoparticles.[12] During the thermal oxidation experiments,[11] a small decrease in electrical mobility diameter was consistently observed when the particles were heated in an unreactive gas (either N_2 or Ar) to temperatures greater than ~350−400 °C. This temperature range is consistent with reports of hydrogen evolution from silicon nanoparticles,[13] porous silicon,[14] and extended crystalline silicon surfaces.[15]

Although the particles produced by the technique used here (a nonthermal RF plasma method) were previously thought to be hydrogen-terminated, a detailed examination of the pristine surface chemistry as a function of temperature has not been reported until now. In this contribution, a method of characterizing the surface chemistry of aerosolized Si nanoparticles is

† Department of Mechanical Engineering.
‡ Department of Chemistry.

(1) Hua, F.; Erogbogbo, F.; Swihart, M. T.; Ruckenstein, E. *Langmuir* **2006**, *22*, 4363.
(2) Nayfeh, M. H.; Rogozhina, E. V.; Mitas, L. In *Synthesis, Functionalization and Surface Treatment of Nanoparticles*; Baraton, M.-I., Ed.; American Scientific Publishers: Stevenson Ranch, CA, 2003; p 173.
(3) Ding, Y.; Dong, Y.; Bapat, A.; Deneen, J.; Carter, C. B.; Kortshagen, U. R.; Campbell, S. A. *Proc. SPIE-Int. Soc. Opt. Eng.* **2005**, 6002.
(4) Roca i Cabarrocas, P.; Chaabane, N.; Kharchenko, A. V.; Tchakarov, S. *Plasma Phys. Controlled Fusion* **2004**, *46*, B235.
(5) Buriak, J. M. *Chem. Rev.* **2002**, *102*, 1271.
(6) Rogozhina, E.; Belomoin, G.; Smith, A.; Abuhassan, L.; Barry, N.; Akcakir, O.; Braun, P. V.; Nayfeh, M. H. *Appl. Phys. Lett.* **2001**, *78*, 3711.
(7) Bent, S. F. *Surf. Sci.* **2002**, *500*, 879.
(8) Wang, G. T.; Mui, C.; Musgrave, C. B.; Bent, S. F. *J. Am. Chem. Soc.* **2002**, *124*, 8990.
(9) Rader, D. J.; McMurry, P. H. *J. Aerosol Sci.* **1986**, *17*, 771.
(10) Kuhn, T.; Krudysz, M.; Zhu, Y.; Fine, P. M.; Hinds, W. C.; Froines, J.; Sioutas, C. *J. Aerosol Sci.* **2005**, *36*, 291.
(11) Liao, Y. C.; Nienow, A. M.; Roberts, J. T. *J. Phys. Chem. B* **2006**, *110*, 6190.
(12) Liao, Y. C.; Roberts, J. T. *J. Am. Chem. Soc.* **2006**, *128*, 9061.
(13) Biswas, R.; Pan, B. C. *Mater. Res. Soc. Symp. Proc.* **2004**, *808*, 65.
(14) Gupta, P.; Colvin, V. L.; George, S. M. *Phys. Rev. B* **1988**, *37*, 8234.
(15) Niwano, M.; Terashi, M.; Kuge, J. *Surf. Sci.* **1999**, *420*, 6.

10.1021/ja0658970 CCC: $37.00

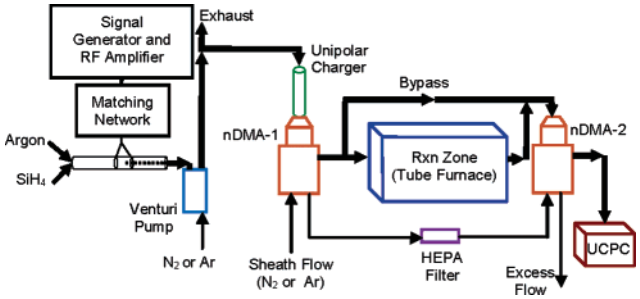

Figure 1. Experimental setup for particle synthesis and mobility measurements.

described. The particle surface composition as a function of temperature is evaluated using both Fourier transform infrared spectroscopy (FTIR) and static time-of-flight secondary ion mass spectroscopy (ToF-SIMS). Effects of temperature on particle morphology, as monitored by transmission electron microscopy (TEM) are described. A concomitant relationship between electrical mobility diameter, morphology, surface chemistry, and temperature is also presented.

Experimental Section

Hydrogen-terminated silicon nanoparticles were produced in an RF plasma using a method similar to that outlined by Mangolini et al.[16] Crystalline particles were produced by this technique, as demonstrated in that report and elsewhere.[12,17] Briefly, particle synthesis proceeded as follows. SiH_4 (0.5% in Ar) obtained from BOC Edwards was mixed with ultrahigh purity argon (Praxair, St. Paul, MN) before being introduced into a low-pressure, nonthermal, quartz tube plasma reactor. Gas flows were 5−10 sccm of the SiH_4/Ar mixture and 400 sccm of ultrahigh purity Ar. RF power at 13.56 MHz was coupled to a 10-mm i.d. (12-mm o.d.) quartz tube reactor using two ring electrodes and a matching network as shown in Figure 1. The RF amplifier was an Electronics & Innovation model A150, and the signal generator was a Tektronics AFG3021. Power output from the amplifier was approximately 30 W.

Silicon nanoparticles were formed at a plasma pressure of ∼20 Torr. The pressure was controlled using one of two methods, depending on the particular analysis technique. For FTIR measurements and ToF-SIMS sample collection, a model 1400 Welch vacuum pump was used. An Air-Vac model UV143H two-stage venturi pump was used in conjunction with mobility measurements. The venturi pump also served as the means by which the particles were brought from the plasma operating pressure up to atmospheric pressure. Essentially, the venturi pump created a low-pressure region by quickly forcing a large volume of gas through a small diameter passage. A port tapped into the small diameter passage served as the vacuum source. This port was coupled directly to the plasma reactor tube, allowing the plasma to run at ∼20 Torr. Particles flowing from the plasma through the venturi pump became entrained in the rapidly flowing gas and were diluted, thus minimizing coagulation. The aerosolized particles in the venturi pump exhaust flow were vented to a larger diameter atmospheric pressure exhaust line from which the aerosol sample was extracted. Gas vent lines from either liquid argon or liquid nitrogen cylinders (Praxair) were used to obtain the volumetric flow rates required to reach the desired pressure.

Changes in particle mobility diameter as a function of temperature were measured using the TDMA apparatus shown schematically in Figure 1. Both DMAs were model 3085 nano DMAs (TSI, Inc., Shoreview, MN), and the particle counter was an ultrafine condensation particle counter (UCPC) model 3025A (TSI). A unipolar aerosol diffusion charger similar to one developed by Chen and Pui[18] was used to produce the charged particles required for mobility classification. Flow rate ratios in the TDMA apparatus were maintained at 10:1. Sheath and aerosol gases were identical for each set of measurements to avoid potential diffusiophoretic effects[19] and further restricted to either nitrogen or argon to minimize reactions between carrier gas and pristine silicon nanoparticles. Electrode voltages were calculated using room temperature air properties. No modifications were made for viscosity, mean free path, or slip correction when switching between nitrogen and argon.

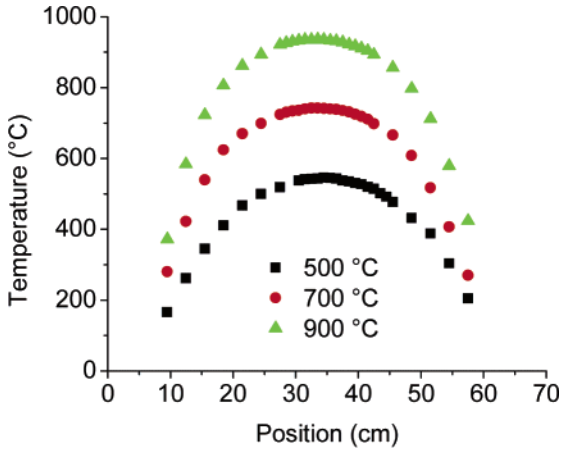

Figure 2. Tube furnace temperature profiles for three different furnace settings. Profiles were measured with a sheathed k-type thermocouple and 1 lpm nitrogen flow to replicate aerosol flow reactor operating conditions.

The TDMA measurements described here were obtained as follows. Aerosol flow was extracted from the atmospheric pressure venturi pump exhaust at 1 L/min in a direction perpendicular to the main exhaust flow. Sampling in this configuration may be considered anisokinetic and could result in a particle size distribution slightly different from that produced by the plasma. However, although the apparatus can certainly be adjusted to make isokinetic sampling feasible, the intent here was not to accurately measure particle size distributions produced by the plasma. As such, the current configuration allowed sampling of a sufficient number of particles so that mobility diameter changes due to thermal processing could be examined. The aerosol sample was immediately introduced into the unipolar charger where particles acquired at most a single charge. (Multiple charging is not expected to occur for particles of diameter less than 20 nm.) For these experiments, positively charged particles were selected for analysis. The aerosol was then directed into the first nDMA, where by adjusting the applied voltage, particles of a specific narrow electrical mobility band were selected for analysis. Those particles selected by the first nDMA were passed through either a single zone tube furnace (Lindberg/Blue model HTF 55122A) or an equivalent length bypass line into the second nDMA. Tubes used in the furnace were either 12-mm o.d. (10-mm i.d.) quartz or 12.7-mm o.d. (11-mm i.d.) Inconel 600. Furnace settings ranged from room temperature to 950 °C. Representative furnace temperature profiles are shown in Figure 2. Radiation heating effects were examined in a previous report using shielded and unshielded type k thermocouples.[20] No significant temperature profile differences were found between shielded and unshielded measurements.

The second nDMA electrode voltage was incrementally stepped over the range of particle mobilities, and particle number concentrations were measured at each voltage with the UCPC. Those number concentration

(16) Mangolini, L.; Thimsen, E.; Kortshagen, U. *Nano Lett.* **2005**, *5*, 655.
(17) Jurbergs, D.; Rogojina, E.; Mangolini, L.; Kortshagen, U. *Appl. Phys. Lett.* **2006**, *88*, 233116.
(18) Chen, D. R.; Pui, D. Y. H. *J. Nanopart. Res.* **1999**, *1*, 115.
(19) Karg, E.; Dua, S. K.; Ferron, G. A. *J. Aerosol Sci.* **1992**, *23*, S389.
(20) Higgins, K. J.; Jung, H.; Kittelson, D. B.; Roberts, J. T.; Zachariah, M. R. *J. Phys. Chem. A* **2002**, *106*, 96.

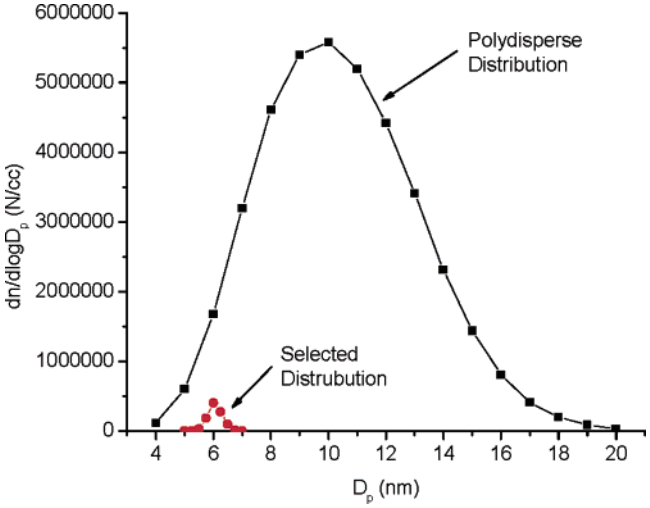

Figure 3. Typical polydisperse distribution prior to mobility selection and a selected distribution corresponding to 6-nm particles.

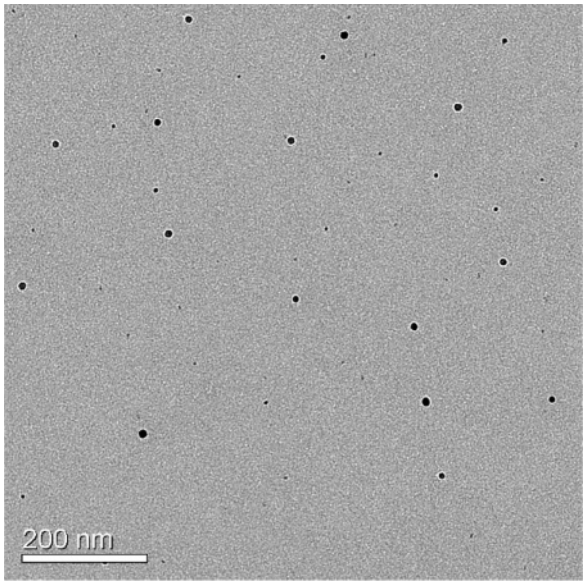

Figure 4. TEM images showing particles collected from the venturi pump exhaust without mobility classification. Particles are discrete and essentially spherical.

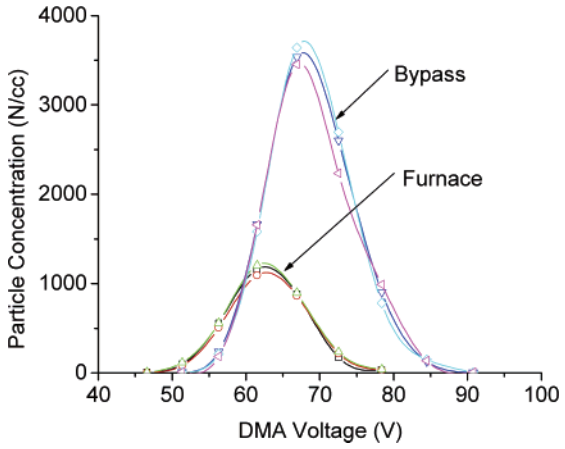

Figure 5. Particle number concentration distributions at 500 °C in nitrogen.

measurements were combined to form representative particle mobility diameter distributions. A normal Gaussian curve was fit to each distribution using the Levenberg−Marquardt algorithm, and the center of each fitted curve was denoted as the equivalent mobility diameter. At each furnace temperature setting, particle distributions from both the bypass and the furnace were measured a minimum of three times and averaged.

Particle surface composition as a function of temperature was characterized using an FTIR spectrometer and static ToF-SIMS. FTIR spectra were obtained in the transmission mode using a Magna-IR, model 550 Spectrometer. With the plasma off, the FTIR spectrometer readily detected SiH_4 in the SiH_4/Ar gas mixture over a path length of 15 cm. With the plasma on, however, no statistically meaningful signal from the SiH_4 or the Si nanoparticles was detected over the same length. Therefore, to characterize the pristine nanoparticle surface chemistry without exposure to air, and to minimize particle losses due to diffusion, a small hybrid gas cell was constructed. This technique provided a means of simultaneously analyzing particle surface chemistry while collecting particles for future stability characterization after exposure to various atmospheres.

To collect a sufficient quantity of particles for FTIR analysis, a piece of fine stainless steel (SST) mesh was mounted perpendicular to the aerosol flow between two short sections of stainless steel tube. (Any suitable IR-transparent filter media could work in place of SST mesh.) The tubes were connected with a quick-flange style clamp. ZnSe windows were mounted on the outer end of each tube to seal the apparatus while simultaneously allowing the IR beam to pass through the hybrid gas cell and mesh. Ports were attached to each tube section on opposite sides of the mesh to provide an inlet and outlet through which the particle-laden gas could flow. As the particles from the plasma reactor flowed through the modified gas cell, a thin layer of silicon nanoparticles accumulated on the mesh. Samples were collected on clean pieces of mesh for a minimum of 20 min before final spectra were recorded. Under the flow conditions used here, the average amount of collected mass was ~0.3 mg.

Samples for ToF-SIMS (Charles Evans and Associates, Redwood City, CA) analysis were also collected on SST mesh in a similar manner. However, samples were kept in their as-produced environment during transport to the instrument by sealing the small gas cell with two valves. This was done to minimize adventitious reactions resulting from exposure to ambient air before loading into the ToF-SIMS analysis chamber. The incident ion beam was gallium, chamber pressure for these measurements was approximately 2 (10^{-8}) Torr, and the extraction voltage was 15 kV. Positive ion spectra were recorded.

Polydisperse particles were collected on carbon TEM grids either by use of an electrostatic sampling device or by impaction. A Tecnai T12 transmission electron microscope (FEI Co., Hilsboro, OR) operating at 120 kV was used to obtain particle images.

Results

Typical particle mobility diameter distributions measured with the TDMA apparatus are shown in Figure 3. The diameters in the nonsymmetric overall distribution range from 4 to 20 nm, with the most probable diameter near 10 nm. The 6-nm selected distributions are symmetric. As shown by the TEM images in Figure 4, particles sampled from the polydisperse aerosol are essentially spherical and nonagglomerated. As an indication of repeatability and distribution changes due to thermal processing, number concentration measurements corresponding to 500 °C in nitrogen carrier gas are shown in Figure 5. Measurements from the bypass closely overlap as do those from the furnace. Because the particles examined here are less than 20 nm in diameter, they acquire a single charge at most in the unipolar charger, and therefore the contribution of doubly charged particles to the distributions is unimportant.

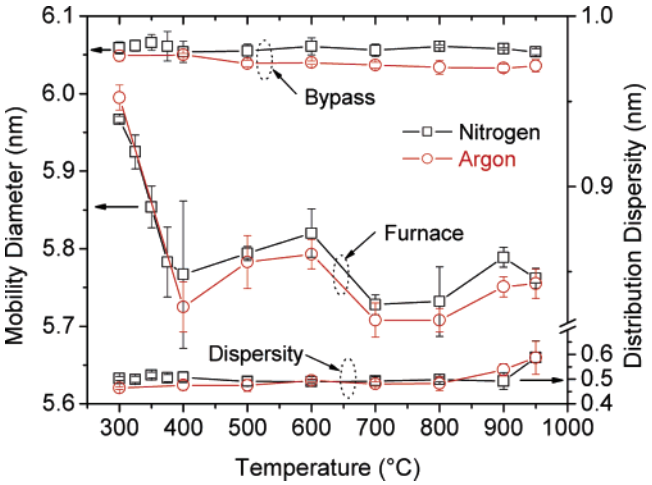

Figure 6. Particle mobility diameter in argon and nitrogen carrier gases as a function of furnace temperature setting. Measurements from the bypass line are nearly constant at approximately 6.05 nm. Dispersity refers to widths of particle distributions passed through the furnace. (fwhm = 1.175 * Dispersity.)

Measured mobility diameter changes as a function of furnace setting are summarized in Figure 6 for particles of 6-nm selected mobility in Ar and N_2 carrier gases. Diameters begin to decrease at 300 °C, and by 400 °C, diameter decreases are 0.25 nm. Although not shown, the same decrease is observed, within experimental error, for 10-nm particles. Between 400 and 600 °C, the change in particle diameter is constant. Above 600 °C an additional decrease occurs, with total shrinkage increasing to 0.3−0.35 nm between 700 and 800 °C. Particles flowing through the bypass line show negligible diameter changes. With the exception of the highest furnace settings studied, distribution dispersity was essentially constant with a distribution full width at half-maximum (fwhm) of ∼0.6 nm.

As shown in Figure 6, mobility diameters measured in nitrogen are generally slightly larger than those measured in argon. However, *differences* in mobility diameter between particles sent through the bypass and those sent through the tube furnace at selected furnace settings are more relevant to the immediate discussion rather than the ultimate TDMA sizing accuracy. If only those diameter differences are considered, then measurements in nitrogen and argon indicate that results are identical, within experimental error. They support the precision of the TDMA apparatus when used to measure very small aerosol size distribution changes in different carrier gases.[21]

Two prominent signals are visible in the FTIR spectra of collected particles, of which representative examples are shown in Figure 7. One of the features is centered near 2100 cm^{-1} and a doublet near 900 cm^{-1}. The region near 2100 cm^{-1}, associated with SiH_x stretching, is shown expanded in Figure 8a for unheated particles and in Figure 8b for particles subjected to processing at 500 °C. The principal peak in Figure 8a is centered near 2113 cm^{-1} with a shoulder near 2141 cm^{-1}. These peaks have been attributed to stretching vibrations of SiH_2 and SiH_3, respectively.[22] A less distinct contribution from the SiH stretch vibration is also present near ∼2095 cm^{-1}. At higher furnace temperature settings, the contributions from SiH_3 and

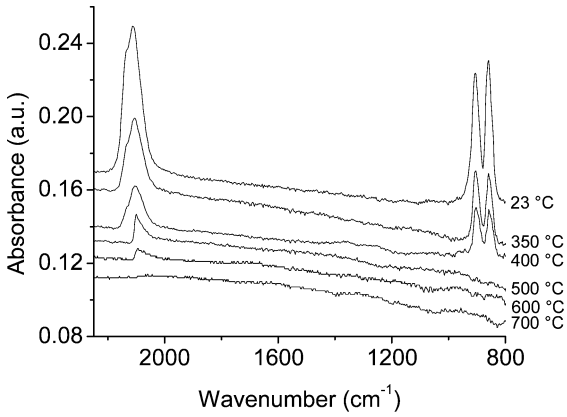

Figure 7. FTIR spectra of silicon nanoparticles as a function of furnace temperature setting.

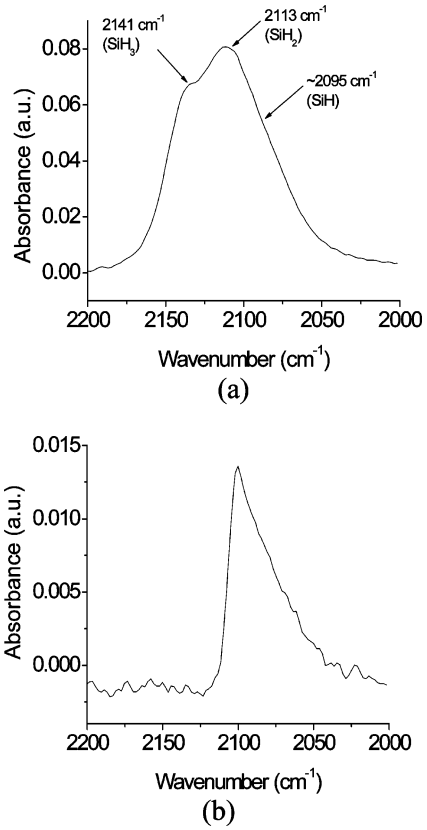

Figure 8. Expanded views of FTIR spectra. (a) Si−H_x stretch region for unheated particles and (b) particles subjected to 500 °C. Note the much smaller signal-to-noise ratio in (b).

SiH_2 rapidly diminish until between 400 and 500 °C the spectrum is composed of various small contributions likely attributable to different SiH configurations.[23,24] Because the particles considered here are essentially spherical, small facets of different crystalline surfaces and transition regions between those facets present opportunities for numerous SiH_x structures. Any disorganized surface content further complicates assignment of the remaining narrow SiH stretch peak to specific structural configurations.

The doublet near 900 cm^{-1}, shown expanded in Figure 9, is associated with the bend-wag deformation modes of the SiH_2

(21) Schmid, O.; Trueblood, M. B.; Gregg, N.; Hagen, D. E.; Whitefield, P. D. *Aerosol Sci. Technol.* **2002**, *36*, 51.
(22) Marra, D. C.; Edelberg, E. A.; Naone, R. L.; Aydil, E. S. *J. Vac. Sci. Technol., A* **1998**, *16*, 3199.
(23) Chabal, Y. J. *Physica B* **1991**, *170*, 447.
(24) Ogata, Y. H.; Kato, F.; Tsuboi, T.; Sakka, T. *J. Electrochem. Soc.* **1998**, *145*, 2439.

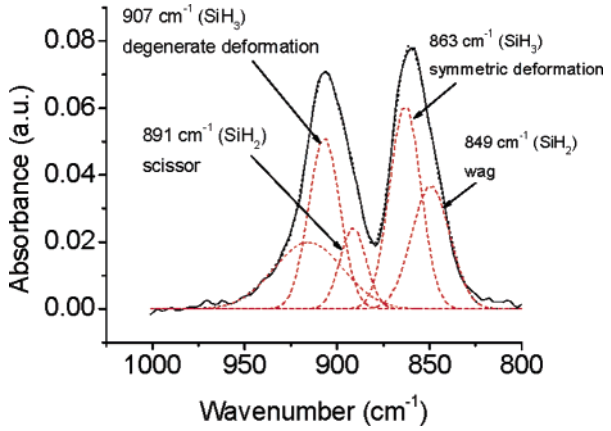

Figure 9. FTIR spectra in the Si−H_x deformation region for unheated particles.

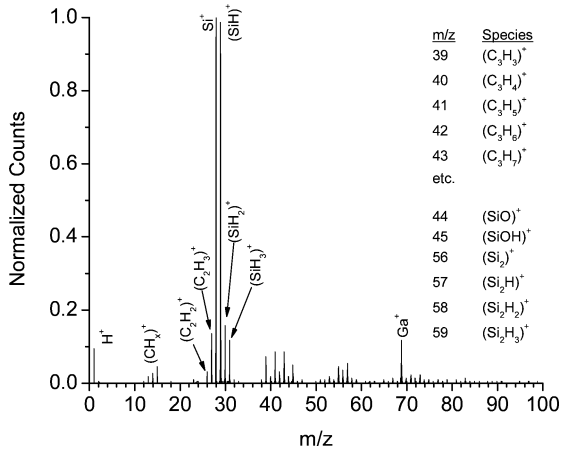

Figure 10. Positive ion ToF-SIMS spectra of unheated particles. All peaks normalized with respect to $m/z = 28$.

and SiH_3 species.[22] Upon closer inspection, two sets of doublets are present. The first set has been attributed to the SiH_2 scissors and wag deformation modes with peaks occurring at 891 and 849 cm^{-1}, respectively. The second set has been assigned to the degenerate and symmetric deformation modes of SiH_3 with peaks occurring at 907 and 863 cm^{-1}, respectively. Between 400 and 500 °C, contributions from the bend-wag deformation modes disappear as shown in Figure 7. Their absence correlates well with the disappearance of peaks in the stretch region attributed to SiH_2 and SiH_3 groups.

ToF-SIMS results shown in Figures 10 and 11 are generally consistent with the FTIR results. In all spectra, the dominant hydrogen-related signal is due to SiH ($m/z = 29$) while contributions from SiH_2 and SiH_3 are much smaller. Nevertheless, the SiH_x peaks decrease in relation to the Si peak ($m/z = 28$) as the furnace setting is increased, demonstrating that surface hydride concentration decreases with increasing furnace temperature. A much smaller hydrogen ion peak also exists, but the intensity does not appear to correlate with the decrease in the SiH-related peaks. Numerous small extrinsic hydrocarbon (C_xH_y) peaks and a less prominent oxide-related peak also appear in the ToF-SIMS spectra. Because the corresponding extrinsic signals do not appear in the FTIR spectra, their appearance may be attributed to ambient air exposure while the samples were transferred from the collection apparatus to the ToF-SIMS sample holder.

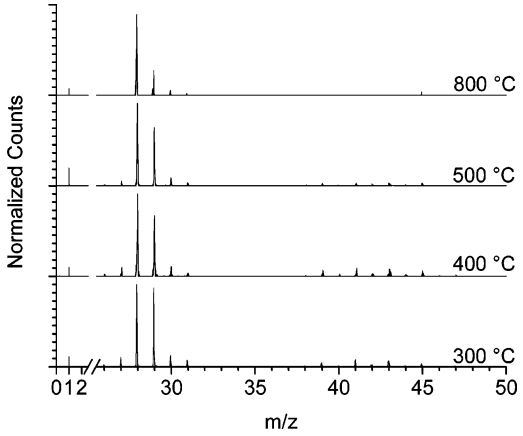

Figure 11. Positive ion ToF-SIMS spectra of heated particles. All peaks normalized with respect to $m/z = 28$.

There are several possibilities for the relatively weak SiH_2 and SiH_3 features in the ToF-SIMS spectra. ToF-SIMS is inherently a destructive technique. The collision cascade caused by heavy ion impact could induce changes in the surrounding surface structure especially if highly strained bonding configurations exist in the particles. The FTIR technique as applied here does not suffer from this destructive characteristic. FTIR and ToF-SIMS spectra have also been compared side by side in a report by Benninghoven et al. regarding the repeatable production of porous silicon.[25] (Porous silicon exhibits complex surface structure akin to that on nanoparticles produced by the method used here: that is, surface termination with SiH_x groups in diverse orientations.[26]) The FITR spectra in that report also implied that SiH_2 was more prevalent than SiH or SiH_3, while in the ToF-SIMS spectra, SiH peaks were more abundant. No reasons were suggested for the differences. In regard to the ToF-SIMS technique, the ionization potential of SiH (~7.9 eV) is less than the ionization potential of both SiH_2 (~8.9 eV) and SiH_3 (~8.7 eV).[27] SiH should therefore exhibit a higher ion yield than SiH_2 or SiH_3. Because of the air exposure during transfer to the ToF-SIMS apparatus and the inherently destructive nature of the technique, the FTIR results probably more closely represent the true pristine particle surface chemistry. However, the ToF-SIMS spectra still qualitatively demonstrate that the particles lose hydrogen as they are processed to higher temperatures and that higher hydride species lose hydrogen first.

Particle mobility diameter changes correlate well with the disappearance of hydrogen-related peaks in the FTIR spectra. The majority of the particle shrinkage occurs by ~400 °C, above which point higher hydride contributions to the FTIR spectra are essentially absent. Although the complete disappearance of the SiH_2- and SiH_3-related peaks occurs at a slightly higher temperature than the initial major particle shrinkage, it should be noted that particle residence time in the tube furnace was somewhat different for the two test conditions. For the TDMA-based size measurements, the flow entering the 10-mm i.d. tube was 1 lpm at atmospheric pressure. The residence time in the furnace for the FTIR results was somewhat less since the flow entering the furnace was 410 sccm at ~20 Torr through an 11-

(25) Sperveslage, G.; Grobe, J.; Egbers, G.; Benninghoven, A. *Fresenius' J. Anal. Chem.* **1998**, *361*, 554.
(26) Buriak, J. M. *Chem. Rev.* **2002**, *5*, 1272.
(27) Joshipura, K. N.; Vinodkumar, M.; Antony, B. K.; Mason, N. J. *Eur. Phys. J. D* **2003**, *23*, 81.

mm i.d. tube. This residence time difference could account for the minor discrepancy between the temperature range at which the majority of the size changes occur and the complete disappearance of the higher hydride signals. A slightly larger diameter decrease occurring between 600 and 700 °C coincides with the disappearance of the SiH stretch contribution in the FTIR spectra. Finally, a slight size increase is exhibited for the highest temperatures. This increase is likely a result of material released from the SST tube adsorbing to the particles.

Attempts were also made to readsorb hydrogen to the particle surfaces by first passing the polydisperse flow through an identical tube furnace set at 400 °C. From those thermally pretreated aerosol distributions, particles of specific mobility diameter were selected by the first nDMA. Immediately downstream from the first nDMA, a small amount of hydrogen was introduced into the carrier gas. This mixture was then allowed to flow through the remainder of the TDMA apparatus and subsequently characterized for apparent mobility diameter changes. No lateral shifts in the distributions were observed, implying that hydrogen did not readsorb to the particles. This result is perhaps not surprising given the low dissociative sticking coefficients that have been reported for hydrogen on single crystal silicon surfaces.[28]

Because the subject of light emission from silicon nanoparticles is also of broad interest, a few brief comments regarding photoluminescence behavior as a function of thermal processing are offered. Upon ultraviolet illumination, particles subjected to room-temperature processing emitted visible red light. As the particles were subjected to increasing furnace temperatures, the photoluminescent behavior changed. Red light was still visible for processing temperatures up to ~500 °C, but between 400 and 500 °C the intensity dropped significantly. When particles were subjected to temperatures greater than ~600 °C, no emission was detectable by eye.

Discussion

The question naturally arises: Why do the particles shrink in the high-temperature furnace? Nanoparticles could shrink due to thermal processing for various reasons. One possible reason is restructuring of amorphous content.[29] The spectra shown in Figure 7 exhibit some similarity to those from a-Si:H thin films.[30] On the other hand, IR spectra of highly crystalline particles[17] appear strikingly similar both to those presented here and to the a-Si:H films. Although the plasma particle synthesis technique is known to produce highly crystalline particles,[12,16,17] there could be some disorganized fraction comprising the particles, even if just an outer layer. Hofmeister et al. studied thermal annealing effects on amorphous silicon (a-Si) nanopowders using high-resolution transmission electron microscopy (HRTEM).[29] After annealing the particles for ~1 h at temperatures from 300 to 600 °C, they found no significant structural or surface roughness changes in the amorphous particles. Annealing for 1 h at 700 °C produced distinct crystalline regions, and at 900 °C almost completely crystalline particles were observed. However, the authors stated that no considerable particle size changes, surface roughness, or increased agglomeration was observed. Since the crystallization time scales in the HRTEM experiments were much greater than the time particles examined here spent in the tube furnace, restructuring of a disorganized or amorphous outer layer is not likely to be the reason for the observed shrinkage occurring around 400 °C.

Even though no apparent size or surface roughness changes were observed by Hofmeister et al. using HRTEM, size changes observed here are near the resolution limit of most TEMs.[31] Mobility diameter measurements using the TDMA apparatus, on the other hand, are sensitive to changes in particle shape.[32,33] However, as shown in the bright field images of Figure 12, particles processed at room temperature appear essentially the same as particles processed at 500 °C. While subtle shape factor changes leading to small mobility diameter shifts cannot be entirely ruled out, particle shape changes were not apparent in Figure 12, nor were they observed elsewhere during in situ heating experiments while being monitored by HRTEM.[21] Quantifying subtle particle shape changes is a formidable task and is beyond the capacity of the techniques available here.

Alternative to thermal restructuring phenomena, desorption of various surface species such as hydrogen[13] and/or poly(silicon) hydrides[34] could be responsible for the observed size decreases. Desorption of surface volatiles could be enough to produce detectable mobility diameter changes, but it could simultaneously allow structural relaxation at particles surface as well (vide infra).

Biswas and Pan examined hydrogen evolution from silicon nanocrystals in an amorphous matrix using molecular dynamics simulations.[13] Their report indicated two hydrogen evolution peaks: the first occurred at ~400 °C and the second between 700 and 800 °C. They attributed the low-temperature peak to hydrogen evolution from the nanocrystal surface and the high-temperature peak to dilute hydrogen evolving from the amorphous matrix. However, they did not specifically report effects due to SiH_3. Other groups[35] have also observed two-peak hydrogen desorption spectra from amorphous silicon nanoparticles using differential scanning calorimetry, albeit the peaks were much closer than those simulated by Biswas and Pan. They attributed the lower-temperature peak (~300 °C) to hydrogen desorption from near-surface regions or surfaces of internal voids. Their explanation of the higher-temperature peak (~410 °C) was that, as a result of restructuring after the low-temperature desorption, the material became more compact, and therefore the desorption process was diffusion-controlled. The authors did not report data for temperatures above 600 °C.

For a-Si:H films grown "on the edge of crystallinity",[36] two hydrogen evolution peaks were also observed: one at ~400 °C and another at ~600 °C. The authors attributed the low-temperature peak to the presence of very small Si crystals in the amorphous matrix which readily allowed H_2 to diffuse to the sample surface along the grain boundaries. The higher-

(28) Doren, D. J. In *Advances in Chemical Physics*; Prigogine, I., Rice, S. A., Eds.; Wiley & Sons: New York, 1996; Vol. 95.
(29) Hofmeister, H.; Dutta, J.; Hofmann, H. *Phys. Rev. B* **1996**, *54*, 2856.
(30) Marra, D. C.; Edelberg, E. A.; Naone, R. L.; Aydil, E. S. *Appl. Surf. Sci.* **1998**, *133*, 148.
(31) Williams, D. B.; Carter, C. B. *Transmission Electron Microscopy*; Plenum Press: New York, 1996.
(32) Hinds, W. C. *Aerosol Technology: Properties, Behavior, and Measurement of Airborne Particles*, 2nd ed.; Wiley: New York, 1999.
(33) DeCarlo, P. F.; Slowik, J. G.; Worsnop, D. R.; Davidovits, P.; Jimenez, J. L. *Aerosol Sci. Technol.* **2004**, *38*, 1185.
(34) Gates, S. M.; Kunz, R. R.; Greenlief, C. M. *Surf. Sci.* **1989**, *207*, 364.
(35) Farjas, J.; Das, D.; Fort, J.; Roura, P.; Bertran, E. *Phys. Rev. B* **2002**, *65*, 115403/1.
(36) Mahan, A. H.; Beyer, W.; Williamson, D. L.; Yang, J.; Guha, S. *Philos. Mag. Lett.* **2000**, *80*, 647.

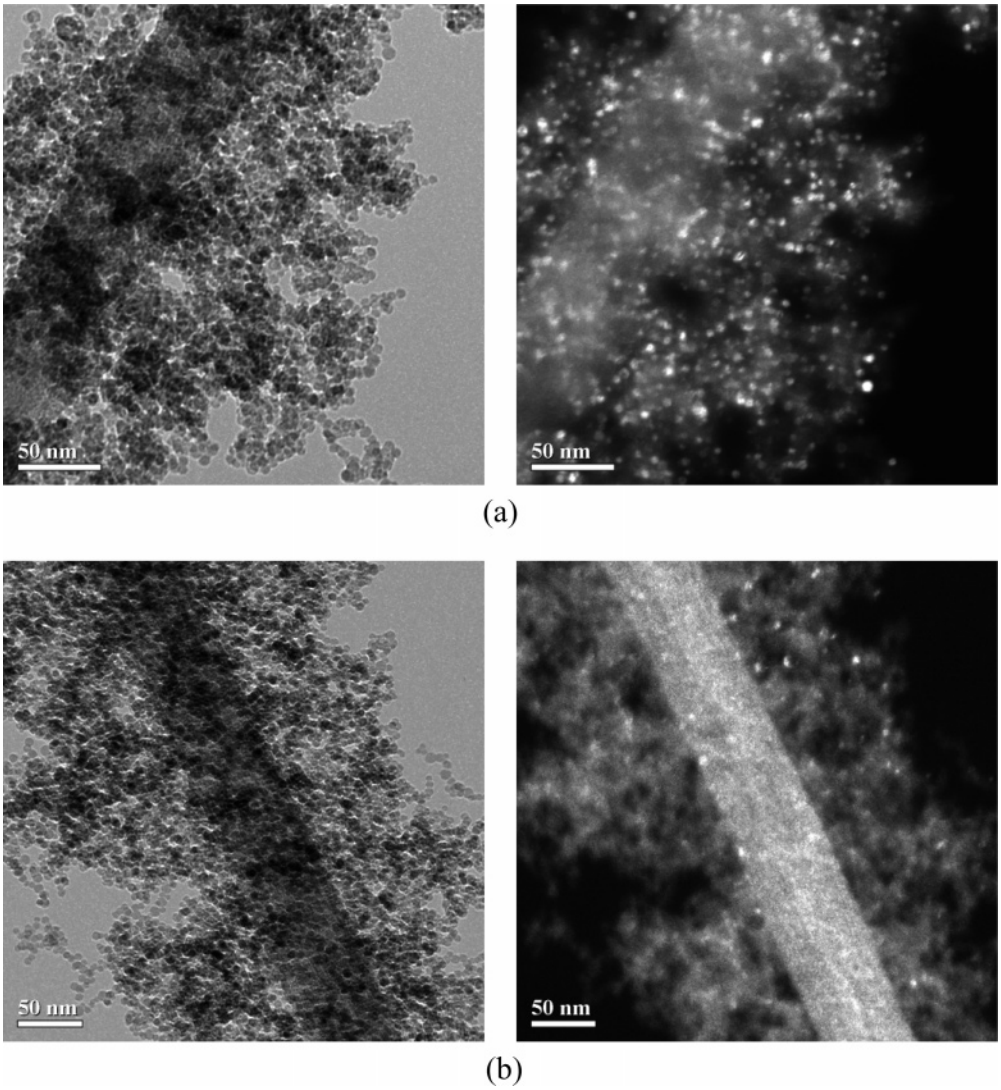

Figure 12. Bright field (left) and the corresponding dark field (right) TEM images of size-polydisperse particles collected electrostatically from the aerosol stream immediately downstream from the tube furnace at ~20 Torr. (a) Particles processed at room temperature. (b) Particles processed at 500 °C.

temperature peak was related to hydrogen diffusion from the bulk a-Si:H film.

Desorption of various silicon hydrides could also lead to the observed particle size changes. Gates et al. used TPD and SSIMS to monitor evolution of hydrogen and silicon hydrides from the Si(100) surface.[34] They found a correlation between the presence of SiH_3 and silane desorption: the SiH_3 either decomposed into SiH_2 and SiH or evolved as SiH_4 at 350−375 °C. A maximum of 4% of the hydrogen desorbed as silane, thus removing about 1% of a monolayer of silicon. This temperature range is consistent with the regime where most of the particle shrinkage occurs but is approximately 50 °C less than the low-temperature molecular hydrogen desorption peak from SiH_2 indicated in their results. Both the FTIR spectra in Figure 7 and ToF-SIMS spectra in Figures 10 and 11 indicate the presence of SiH_3 which could promote silane desorption, thus producing the observed size changes. Gates et al. also observed desorption of poly(silicon) hydrides occurring at temperatures co-incident with the low-temperature H_2 desorption peak due to SiH_2 decomposition around 425 °C. However, the quantity of desorbed poly(silicon) hydrides was significantly less than the amount of desorbed H_2. Similar desorption phenomena could occur in the particles examined here, thus contributing to the observed size changes. Desorption of significant amounts of SiH_4 and/or Si_xH_y, however, is likely to result in particle mobility diameter decreases much larger than that observed here.

These reports suggest two desorption regimes exist, both of which correlate fairly well with the results presented here: a lower-temperature range where hydrogen most readily desorbs as H_2, and a higher-temperature range where more dilute or isolated hydrogen probably evolves. Temperature ranges of these simulations and experiments correlate fairly well with the FTIR results and may be used to explain the observed mobility diameter changes for temperatures up to ~600 °C. Perhaps the most plausible explanation of the initial shrinkage is that the diameter changes are primarily a result of molecular hydrogen desorption from SiH_2 since the shrinkage occurs at approximately the correct temperature for hydrogen desorption, and the observed changes (approximately 0.25-nm decrease in diameter) match fairly well with the Si−H bond length of ~0.15 nm.[37] Although there is still a small hydrogen signal present in

(37) Chang, K. J.; Chadi, D. J. *Phys. Rev. B* **1990**, *42*, 7651.

the FTIR spectra at 600 °C, it is possible that the Si−H bonds are not oriented normal to the particle surfaces and/or could be providing a particle structure stabilizing effect. To explain the slightly larger mobility diameter decrease for temperatures greater than 600 °C, silicon nanostructure simulations are considered.

Yu et al.[38] used a molecular dynamics simulation to study properties of silicon nanostructures covered with different amounts of surface hydrogen. By simulating a 1000 K environment and subsequent cooling to 0 K, they found that fully hydrogen-terminated surfaces enabled nanostructures to retain their original bulk crystalline structure. Only a small lattice contraction of 0.01 to 0.02 Å was observed in the outermost 2−3 layers, and an even smaller lattice expansion was simulated for the interior of the cluster. However, for crystalline nanostructures with incomplete hydrogen termination, the trend was for the bulk tetrahedral configuration to become more distorted as more hydrogen was removed. For example, annealing a structure with ∼50% surface hydrogen coverage allowed the interior tetrahedral structure to remain essentially intact. However, removing 70−80% of the surface hydrogen caused structures to develop a more compact form no longer exhibiting the preannealed crystalline structure. No overall size changes were reported. Although quantitative determination of nanoparticle hydrogen coverage from FTIR or ToF-SIMS spectra is not straightforward, Figures 7 and 11 suggest that very little hydrogen exists on the particles for temperatures above 600 °C. Therefore, based on the molecular dynamics simulations by Yu et al.,[38] the conclusions of which are consistent tight-binding calculations by the same group,[39] restructuring to a more compact, noncrystalline forms may be occurring as a result of decreasing hydrogen concentration. This could account for increased shrinkage at temperatures greater than 600−700 °C where the hydrogen content is significantly lower than at room temperature.

Experimental evidence supporting the restructuring explanation is shown in Figure 12 where bright spots in the dark field images are suggestive of crystalline material. As shown in the images, the number of bright spots is much greater for particles processed at room temperature than for particles processed at 500 °C. This implies that particle crystallinity is decreasing as a result of elevated temperature processing. According to the FTIR results, particles processed at 500 °C contain very little hydrogen. Based on the results presented by Yu et al.,[38] therefore, restructuring to more compact forms could be occurring. Loss of crystallinity could also partially explain the photoluminescent behavior changes associated with increased processing temperature.

(38) Yu, D. K.; Zhang, R. Q.; Lee, S. T. *J. Appl. Phys.* **2002**, *92*, 7453.
(39) Yu, D. K.; Zhang, R. Q.; Lee, S. T. *Phys. Rev. B* **2002**, *65*, 245417.

Conclusion

The surface chemistry of pristine silicon nanoparticles has been evaluated without ambient air exposure. Effects of thermal processing on the chemistry of hydrogen-terminated nanoparticles produced in a nonthermal RF plasma were evaluated with FTIR, ToF-SIMS, and a TDMA apparatus. FTIR spectra indicated that pristine particle surfaces were primarily covered by SiH_2 groups with smaller amounts of SiH and SiH_3, while ToF-SIMS spectra indicated slightly different surface composition. FTIR results showed that SiH_2- and SiH_3-related signals largely disappeared at temperatures lower than that of SiH. Regardless of the differences, both techniques demonstrated that the surface hydrogen coverage decreased as the processing temperature increased. Heating the particles also produced modest mobility diameter decreases which correlated well with the disappearance of hydrogen signals in the FTIR and ToF-SIMS spectra. Both the surface chemistry and mobility diameter changes reported here are important considerations for techniques used to impart passivation or functionalization layers to the particles if the as-produced particle properties are to be retained.

Acknowledgment. This work was supported in part by the National Science Foundation under Grant No. 0094911, in part by the MRSEC Program of the National Science Foundation under Award No. DMR-0212302, and in part by the IGERT Program of the National Science Foundation under Award No. DGE-0114372.

JA0658970